FT-IR Imaging of Solvent-Induced Crystallization in Polymers

Andreas Gupper, K. L. Andrew Chan, and Sergei G. Kazarian*

Department of Chemical Engineering and Chemical Technology, Imperial College London, South Kensington Campus, London SW7 2AZ, United Kingdom

Received April 8, 2004; Revised Manuscript Received June 14, 2004

ABSTRACT: A novel application of FT-IR imaging to simultaneously study solvent diffusion and solvent-induced crystallization in polymers has been demonstrated. Using a spectroscopic imaging technique, these phenomena were spatially resolved from the polymer/solvent interface to the bulk region of the polymeric material. Image acquisition with a 64 × 64 focal plane array detector in fixed time intervals, integration of specific bands in the FT-IR spectrum, and plotting the distribution of the corresponding integrated band absorbance values over the measured area allowed simultaneous monitoring of the solvent diffusion into the polymer and the related spatial distribution of morphological changes. These in situ experiments were performed in a controlled environment cell (temperature and solvent vapor pressure) with infrared transparent windows. The work was focused on syndiotactic polystyrene due to its scientific interest and technological importance. The type of diffusion and solvent diffusion coefficients for toluene at 20 and 35 °C were determined. Furthermore, conversion of amorphous to δ-crystalline syndiotactic polystyrene was observed, and the dependence of crystallization kinetics on solvent concentration has been described.

Introduction

Solvent diffusion and polymer crystallization are two important and fundamental phenomena in polymer science. They affect many properties and possible applications of polymeric materials and are also encountered in polymerization and processing steps. Therefore, a wide range of analytical techniques have been applied for the investigation of these phenomena. Vibrational spectroscopic methods were primarily employed because of their conformational sensitivity that facilitates investigations on structural changes in polymers. A new and very powerful step forward in the field of vibrational spectroscopy was made by the introduction of Fourier transform infrared (FT-IR) imaging.[1] Conventionally, chemical maps of samples were obtained with FT-IR microscopy by measuring IR spectra at different areas of the sample in a grid pattern. The variation of the absorbance of a specific absorption band that represents a particular component has been plotted as a map. This is achieved by performing a point-by-point mapping with an aperture and a computer-controlled motorized stage and is normally a very time-consuming process. Most importantly, application of the mapping approach prevents studying of dynamic systems. In contrast, FT-IR imaging uses a focal plane array (FPA) detector, which is a large assembly of mercury cadmium telluride (MCT) elements, e.g., 4096 single element detectors in a 64 × 64 array. Therefore, it is possible to simultaneously measure and differentiate between the spatial distribution of composites in a blend[2,3] or even of different morphologies of chemically identical substances, for example, amorphous and crystalline domains in polymers.[4] It was demonstrated recently that the spatial resolution of FT-IR imaging can be as high as 4 μm.[5] Furthermore, measurement times using the imaging approach are relatively short (minutes time scale). This is especially important for studying dynamic processes involved in polymer/solvent interactions.

This work includes syndiotactic polystyrene (s-PS) because of the significant scientific interest and technological importance of the system.[6] Since its first synthesis in the 1980s, this polymer with its complex polymorphic behavior was subjected to intensive studies. When dealing with the semicrystalline s-PS, a principal distinction must be made between the trans-planar α and β modifications and the helical γ and δ forms. The first two modifications are more stable than the latter forms and can be obtained by heat treatment of amorphous raw material. Introduction of γ and δ crystallinity into amorphous s-PS requires the use of a solvent in processes such as precipitation from solution, solvent casting, or exposure to solvents in their liquid or gaseous forms. The definition of a nomenclature for different crystalline forms, which is also used throughout this text, was published by Guerra et al. in 1990,[7] and the conditions for the transformation of crystalline modifications have been reported by Kellar et al.[8] An excellent vibrational spectroscopic background including normal-coordinate analysis of s-PS has been provided by Hsu and Reynolds.[9] The transformation process from amorphous to δ-crystalline s-PS was described in detail for example by Spells et al.[10] and Kaji and co-workers.[11] The most relevant studies to the work described in this paper are by Tashiro et al.,[12−15] who also examined the s-PS/toluene system and studied the introduction of δ-crystallinity using conventional FT-IR spectroscopy. That previous research showed that exposure of amorphous s-PS to organic solvents results in the formation of crystalline phases in s-PS. The key issue in solvent-induced crystallization is whether the rate of crystallization was limited by solvent diffusion. This was difficult to assess using conventional in situ spectroscopy.[12] Indeed, conventional in situ spectroscopic measurements of a free-standing polymer film, which is placed in the transmission cell and exposed to the solvent vapor, yield overall changes to the polymer crystallinity but not the crystallinity profile across the film. The total solvent mass uptake also does not provide spatial distribution to interrelate these phenomena.

* Corresponding author: e-mail s.kazarian@imperial.ac.uk.

10.1021/ma049313v CCC: $27.50
Published on Web 07/31/2004

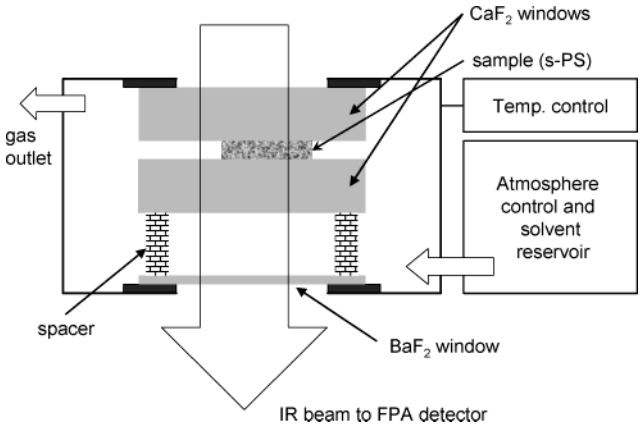

Figure 1. Schematic drawing of the experiment setup: The s-PS film is slightly pressed between two CaF_2 windows to prevent solvent leakage. A thin BaF_2 window and the upper CaF_2 window seal the cell. The atmosphere and temperature in the sample compartment are controlled by an external control unit.

In this work the polymer/solvent interfacial region of s-PS is studied via FT-IR imaging spectroscopy to gain simultaneous information on the spatial distribution of the solvent and the morphology of the polymer. The potential of applying FT-IR imaging to polymeric materials under a controlled environment was illustrated recently.[16,17] FT-IR imaging allows one to measure in transmission mode the relatively large interfacial region (e.g., 400 × 400 μm^2) of the film in contact with the solvent as a function of time. Koenig and co-workers [18−20] have successfully demonstrated the feasibility of such an approach for dissolution of polymers in organic solvents. However, this is the first time that FT-IR imaging was applied in situ to study organic solvent-induced polymer crystallization. The approach demonstrated here is applicable to a wide range of polymers and not limited to s-PS only.

Experimental Section

Samples. The authors thank Dr. Y. P. Handa for supplying a film of amorphous s-PS. For all experiments the dimensions of the sample were about 1 mm × 1 mm × 50 μm. For solvent vapor generation liquid toluene of 99.5% purity, supplied from BDH Laboratory Supplies, UK, was used.

Equipment. FT-IR spectra and images were collected with an IFS 66/S spectrometer coupled to an IRscope II infrared microscope (Bruker Optics). Spectra acquisition was achieved via a MCT single element detector or 64 × 64 FPA detector. Reference spectra of different s-PS modifications were acquired with a wavenumber resolution of 4 cm^{-1} using 50 coadditions on the single element MCT detector. FT-IR images were obtained by using the FPA detector and consist of 4096 single spectra with 8 cm^{-1} resolution (20 coadditions) probing an area of 266 × 266 μm^2. Furthermore, image acquisition was carried out under controlled environments using a VGI 2000M cell (Surface Measurement Systems Ltd., UK). Temperature was set to either 20 or 35 °C, and partial vapor pressure was set to 99.9% of solvent vapor.

Experimental Details. One of the key issues of this work was arranging the experimental setup, which is schematically outlined in Figure 1. It consists of a VGI 2000M cell with IR transparent windows for infrared and visual light transmission and a control system to regulate the temperature and the atmosphere within the sample compartment. In this setup spacer material (Isolast seals) and two thick CaF_2 windows are used to mount and slightly squeeze the thin polymer film. A thin BaF_2 window at the bottom is used together with the upper CaF_2 window to seal the cell against the outer atmosphere. Solvent vapor flowing through the cell reaches the polymer sample via the gap between the two CaF_2 windows only from the side of the film. In this experimental design, the solvent diffusion process within the polymer can be regarded as one-dimensional, along the direction perpendicular to the path of the transmitted infrared beam which is indicated by the arrow pointing downward in Figure 1. Such an arrangement also prevents solvent leakage at the CaF_2 windows/polymer interfaces as was proven by the experimental data. With this arrangement in the FT-IR imaging approach, time- and spatially-resolved information can be obtained to monitor the solvent diffusion and polymer crystallization processes. In previous FT-IR spectroscopic studies,[12] a free-standing polymer film was exposed to solvent vapor, and the probing infrared light beam, perpendicular to the surface of the film but parallel and antiparallel to the direction of solvent diffusion, always registered the overall solvent uptake and the overall change in crystallinity throughout the thickness of the polymer film. Therefore, no distinction was possible between the polymer/solvent interface near region and the center of the polymer film which were affected by the solvent at different times. As will be shown below, the experimental setup has a strong effect on the values obtained for crystallization kinetics.

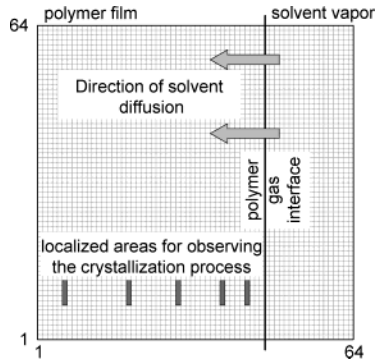

Figure 2. Schematic structure of the 64 × 64 FPA detector. Superimposed is the design of the experiment layout showing the polymer/solvent interface, direction of solvent diffusion, and the selection of pixel used to increase signal-to-noise ratios at unaltered spatial resolution.

Figure 2 illustrates schematically the structure of a FPA detector with its 64 × 64 array of single elements (each square represents one detector element) and the principle of the performed experiments. The position of a single measurement point on the sample can be provided by giving the row and column number of the detector element alternatively to the conventional micrometer coordinates nomenclature in mapping approaches. It is convenient to use the first method as this exactly defines the single detector element within the FPA that registered a specific spectrum and is correlated to a specific point in the image. A black line overlaid on the grid in Figure 2 indicates the polymer/solvent interface. In all experiments the solvent is used in its gaseous state rather than in its liquid state to introduce crystallinity because of the lower solvent concentration at the interface (easier to distinguish the condensed zones within the polymer and the gaseous supply) and the advantage that no polymer dissolution is observed during longer experiments. Toluene vapor supplied from the right side of the line was allowed to diffuse into the amorphous polymer film only in the direction indicated by the two arrows. The bars in the bottom region of Figure 2 should clarify the process of spectrum averaging in order to enhance the signal-to-noise ratios without deterioration of the spatial resolution of the data provided. The drawing demonstrates which neighboring single detector elements were selected for the signal averaging process (the number of pixels varied between different experiments).

Using an FPA detector for FT-IR imaging restricts the accessible spectral range of the IR spectrum to wavenumbers above 900 cm^{-1}. The employment of CaF_2 windows further narrows this region toward higher wavenumbers so that effectively only spectral information in the range from ∼1000

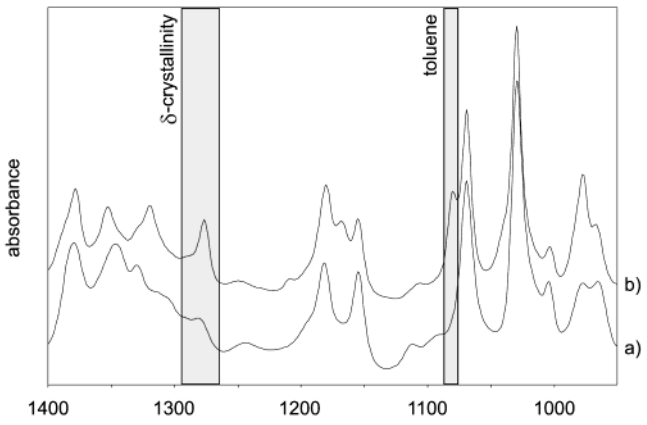

Figure 3. FT-IR reference spectra of (a) an amorphous s-PS film used as starting material and (b) a δ-crystalline s-PS film after exposure to toluene. The wavenumber ranges used to integrate bands specific to the δ-crystalline s-PS and toluene are indicated by gray bars.

to 3950 cm^{-1} can be used for interpretation. This confinement in wavenumber region (compared to conventional IR spectroscopy) is the reason for selecting spectral bands to monitor solvent diffusion and polymer crystallization which are not the same as those reported in previous papers and makes direct comparison with them more difficult. Figure 3 shows reference spectra of amorphous s-PS (spectrum a) and δ-crystalline s-PS obtained by inducing crystallinity with toluene (spectrum b). The gray bars indicate the wavenumber regions selective for the δ-crystallinity of s-PS and toluene. Although several spectral changes can be recognized on introduction of δ-crystallinity (despite the appearance of solvent bands), integration of the band at 1275 cm^{-1}, which has been assigned to a backbone vibration in TTGG conformation, proved most successful for monitoring the crystalline area of the sample. Choosing a band selective for toluene was a much more complicated task. As the structure of styrene, and hence that of the resulting polymer, is very similar to that of toluene most of the vibrational bands in the accessible wavenumber range strongly overlap in the FT-IR spectrum. Only the shoulder centered at 1080 cm^{-1}, a ring δ(CH) vibration, of the much stronger in-plane CH bending vibration of polystyrene centered at 1069 cm^{-1} could be used to image the movement of toluene. Unfortunately, this band is very close to the cutoff edge of the CaF_2 window, and therefore data in the FT-IR images are noisy due to the low transmitted light intensity. Integration of a selective wavenumber region and plotting the integrated absorbance value obtained from each FPA pixel results in FT-IR images such as the ones shown in Figure 4, where the δ-crystalline areas of a polymer film after different solvent exposure times are shown by integration of the 1275 cm^{-1} band. These data reveal that the polymer starts crystallizing at the interface immediately after exposure to solvent vapor and that the crystalline area grows with time. In Figure 4 the same color scale was applied for all images: orange indicates high, green low, and blue no crystallinity at all. The numbers on the right of the scale bar correspond to the integrated band absorbance values. Although the starting material was described to be amorphous, an s-PS sample will always contain some segments in TTGG conformation that account for a certain level of crystallinity related vibrations and only areas without any polymer appear blue in the images. Negative values for the integrated absorbance result from baseline noise which is the only signal contribution after background correction in areas without polymer.

Results and Discussion

Solvent Diffusion Coefficients. As proved by the FT-IR images in Figure 4, visualization of the crystallization process, which is directly related to the solvent diffusion process, is possible with the approach introduced in this work. To extract information about solvent diffusion, the following data plotting method was used. For the same experiment as shown in Figure 4, intensity profiles for the distribution of polymer crystallinity across the FPA are provided in Figure 5. The integrated band absorbance values (of the 1275 cm^{-1} band) are plotted vs the horizontal pixel number of the FPA detector. 10 pixels parallel to the polymer/solvent interface were averaged to increase the signal-to-noise ratio for the determination of the solvent diffusion coefficients. (In the case of Figure 5 the bottom 10 rows of the FPA were averaged.) The values for the calculation of diffusion coefficients and polymer crystallization

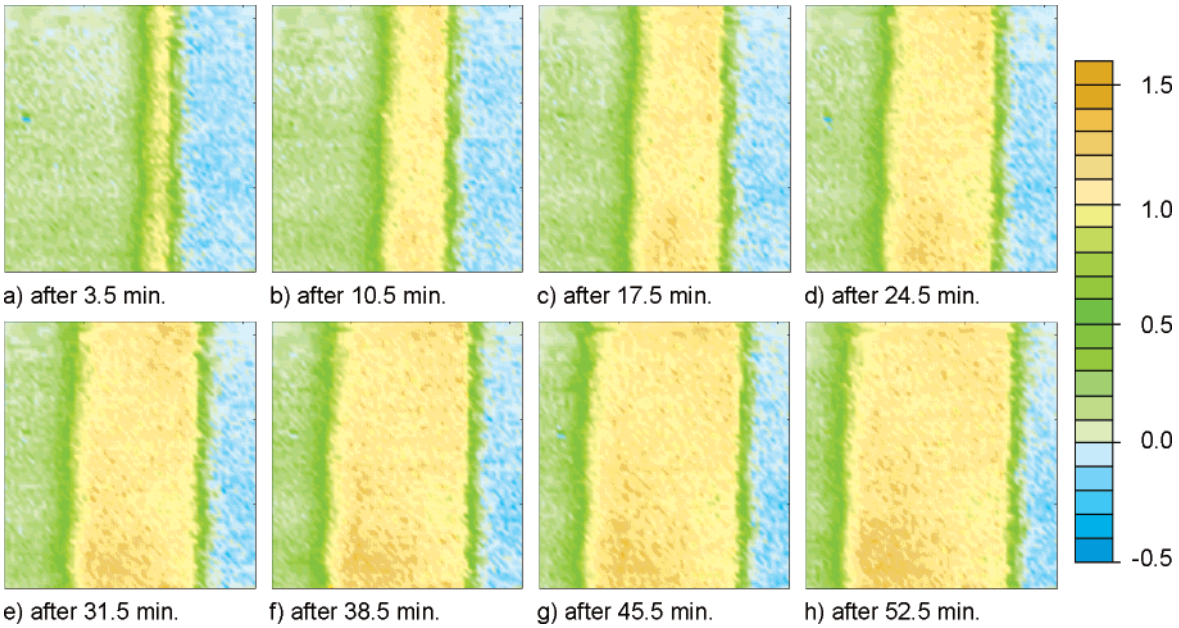

Figure 4. FT-IR images are based on the distribution of the integrated absorbance of the band at 1275 cm^{-1} (δ-crystallinity within the s-PS film) as a function of different solvent exposure times (indicated below the corresponding images). Highly crystalline domains appear orange, and the blue refers to the absence of crystallinity. The scale bar to the right corresponds to the integrated absorbance of the band at 1275 cm^{-1}. The image size is 266 × 266 μm^2.

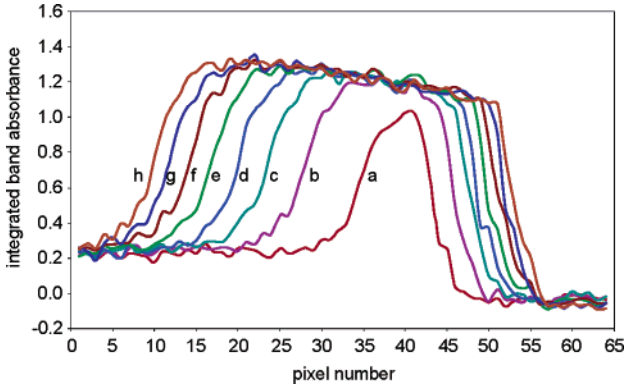

Figure 5. Profiles of the integrated absorbance of the band at 1275 cm^{-1} as solvent exposure time increases vs the horizontal pixel number on the FPA detector. 10 vertical detector elements have been coadded for an enhanced signal-to-noise ratio. The letters a to h refer to the images in Figure 4.

kinetics were extracted from similar plots and by assuming the following arguments to be true:

The position of the polymer film edge can be found by integrating the wavenumber region between 1420 and 1530 cm^{-1} (not included in Figure 3). There, the two strong bands mainly arising from the in-plane bending of the benzene ring are far too strong to be within the linear response limit of the detector but are suited to find the edge of the film. When plotting the integrated absorbance values against the pixel number of the FPA, as demonstrated in Figure 5 to show the δ-crystalline areas, the point at 50% of the highest integrated absorbance value was considered to be the edge of the film.

Creating analogous plots by integrating the solvent band (1080 cm^{-1} for toluene) allows determination of the distances diffused by the solvent. Once again, the points at 50% difference between highest and lowest values were chosen to calculate the distance for the front of solvent.

Polymer swelling, which in Figure 5 can be recognized by the movement of the polymer edge toward higher pixel numbers, has not been taken into account when calculating the diffusion coefficients.

The diffusion process was assumed to occur parallel to the selected row of detector elements.

The plotting method introduced in Figure 5 allowed recovering data to determine whether solvent diffusion shows Fickian, anomalous, or case II behavior. A common way[21] to specify the type of diffusion is to evaluate the diffusion exponent α of eq 1, where d is the solvent front distance from the polymer/solvent interface after a given time t and A is a proportionality factor.

$$d = At^{\alpha} \tag{1}$$

An α value of 1 would imply case II diffusion whereas 0.5 is indicative of Fickian diffusion. After taking the logarithm of eq 1 the diffusion exponent α appears as the gradient of a straight line equation. Thus, α can be obtained from a plot of the logarithm of solvent diffusion front distance (in μm) vs logarithm of solvent exposure time. In Figure 6a the results of experiments with toluene vapor at 20 ($\alpha = 0.59$) and 35 °C ($\alpha = 0.49$) are shown. From them, Fickian diffusion can be assumed for the first 200 μm of toluene diffusion into an s-PS film. To obtain the solvent diffusion coefficients, the

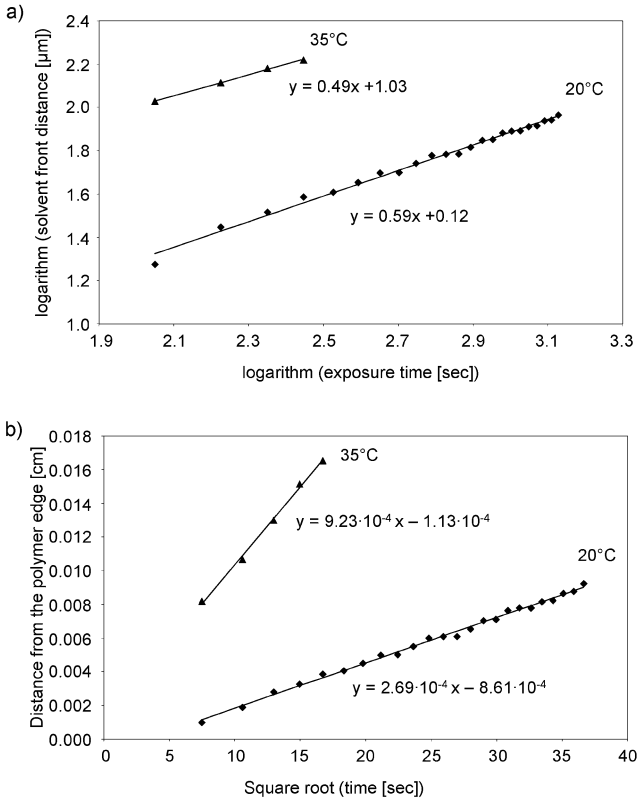

Figure 6. (a) A log−log plot of the distance of the front of toluene obtained from the absorbance profile. This plot allows determination of diffusion behavior of the solvent. (b) Plot of distance of the front of toluene (calculated as a position of 50% of the maximum absorbance for the corresponding band of toluene) as a function of square root of time. This plot allows determination of diffusion coefficients of toluene in s-PS. Diamond dots: experiment at 20 °C; triangles: experiment at 35 °C.

distance of the solvent front from the polymer edge (in cm) is plotted vs the square root of time in Figure 6b. The regression line in this figure is a fit to eq 2, where d again represents the measured distance of the solvent front after time t.

$$d = D^2\sqrt{t} + d_0 \tag{2}$$

The regression line should go through zero at time zero, but the time resolution of the system accounts for the deviation (expressed by d_0) from this desired set point. The slope of the regression line, in eq 2, corresponds to the square of the diffusion coefficient (D). Using the plotting technique introduced in Figure 5, a diffusion coefficient of 7×10^{-8} cm^2 s^{-1} for toluene at 20 °C is obtained. For the same experiment carried out at 35 °C a value of 2×10^{-7} cm^2 s^{-1} can be calculated. The experiments prove the expected dependence of solvent diffusion on temperature. With the current setup lower temperatures were not accessible, and at higher temperature diffusion was too fast to be monitored by our system. The observed behavior is in agreement with previous studies.[12,22]

In regard to the accuracy of the diffusion coefficients, it must be noted that the complex crystallization process, trapping of solvent molecules between the macromolecular chains, and changes in density and morphology depending on the degree of crystallinity[7] account for uncertainties. Also, the time resolution of the system is limited. For all data given, time zero refers

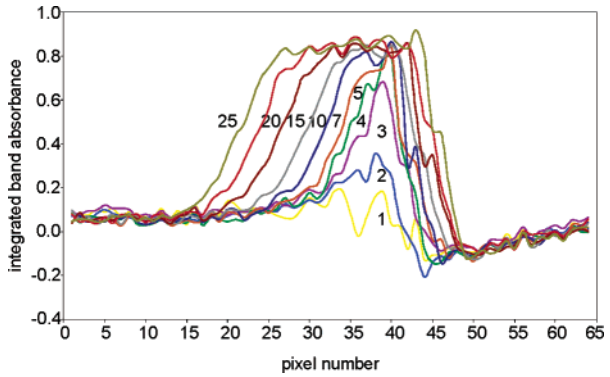

Figure 7. Profiles of the integrated band absorbance of the 1275 cm^{-1} band as solvent exposure time at 20 °C increases. The numbers next to the curves refer to solvent exposure time (in minutes) of the s-PS film. This plot shows the extent of the δ-crystalline areas in the s-PS film.

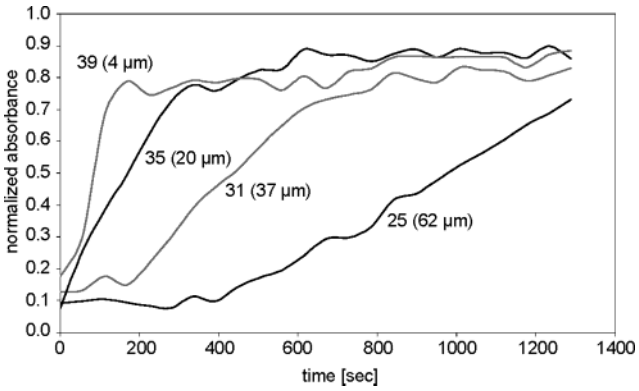

Figure 8. Profiles of the integrated absorbance of the band at 1275 cm^{-1} at various points across the polymer/solvent interface as a function of solvent exposure time. The numbers next to the lines give the corresponding FPA detector pixel number. The calculated distances from the polymer/solvent interface at the start of the experiment (in brackets) are given in micrometers.

to the starting of the solvent flow through the cell, which occurred simultaneously with the start of the first image acquisition. Changes occurring in the sample during the image acquisition process (between 50 and 210 s depending on the registered spectral range) are always associated with the time of starting the imaging process.

Polymer Crystallization Kinetics. Another new aspect of this work is imaging the crystallization process in the polymer/solvent interface near region. As far as we know, this is the first time that the solvent dependence of s-PS crystallization can be spatially resolved by a vibrational spectroscopic technique. The spatial resolution in transmission FT-IR imaging is about 20 μm as estimated from the Rayleigh criterion.[5] In Figure 4 images of the crystalline areas and in Figure 7 integrated band absorbance profiles (of a similar experiment with higher time resolution) for crystalline s-PS are presented after different solvent (toluene) exposure times. From both figures it can be recognized which areas in the film already started to crystallize and to what extent they are affected. The curves in Figure 7 illustrate that the full amount of crystallinity at the interface region is reached after about 4 min. Hence, the crystallization process at 20 °C in the surface near region of the s-PS film is completed much faster than reports in previous papers would suggest[12,13] from measurements of overall changes in the polymer film. The concept of critical sequence lengths, which was provided as an explanation for the time delay of crystallization at the beginning of the experiment (in the order of several minutes), has to be reconsidered. Although the concept is reasonable, the 1275 cm^{-1} band used in the current work does not show the same delay as exhibited by other bands observed by Tashiro and coworkers[12] with similar (12−15 repeat units) or even larger critical sequence lengths. It may well be that in the presence of a sufficient solvent concentration the rearrangement of macromolecular chains happens faster than hitherto reported. From Figure 7 it can also be recognized that the degree of crystallinity at the polymer surface does not change significantly after longer solvent exposure times, which is evidence of two phenomena: first, longer solvent exposition does not result in a higher crystallinity of the polymer, and second, no polymer dissolution takes place when solvent vapors are used.

Of particular interest were spatially resolved measurements of the crystallization kinetics at different distances from the polymer/solvent interface. Figure 8 describes the crystallization process of s-PS registered by different pixels of the FPA detector. In this figure the numbers next to the curves refer to the horizontal pixel number of the FPA detector as indicated in Figure 2, and the approximate distance from the polymer/solvent interface in micrometers before starting the experiment is given in brackets. It can be noticed that at pixel 39 the crystallinity increases slightly slower than evident from Figure 7 and mentioned in the paragraph above. This is due to the fact that in Figure 8 the signal of a single pixel on the FPA detector is plotted rather than the information from a spot at constant distance from the polymer/solvent interface. Close to the interface polymer swelling affects the time needed to complete the crystallization process within the area registered by one specific pixel. There, swelling brings polymer with shorter solvent exposure time (lower crystallinity) from the bulk region of the film into the IR beam registered by the same pixel of the FPA detector element and is in this way responsible for the seemingly slower crystallization process. At positions further away from the polymer edge, swelling still occurs, but the contribution of this effect on the measured crystallization kinetics is less pronounced and is negligible as it becomes smaller than errors arising from the resolution limits of the FT-IR system in terms of lateral dimension and time. When crystallization is considered at distances further away from the polymer/solvent interface, the curves in Figure 8 and also Figure 9 can be separated into three regions (shown for pixel 18 in Figure 9): in the first region no crystallization occurs, and the curve remains flat at a low crystallinity level. Obviously there is not enough solvent present to start the solvent-induced crystallization process. The second region starts with the beginning of the crystallization process and lasts until crystallinity reaches its final value. In the third and last region the curve is flat, indicating that no further changes occur in terms of crystallinity but the solvent concentration in the system may still be increasing. In region two, the slope of the curve is related to the time the system requires to complete crystallization. It is obvious from Figures 8 and 9 that there is a relationship between the distances from the polymer/solvent interface and the time for the s-PS film to reach the final degree of crystallinity. The explanation for this phenomenon could be that the crystallization process is linked to the concentration of

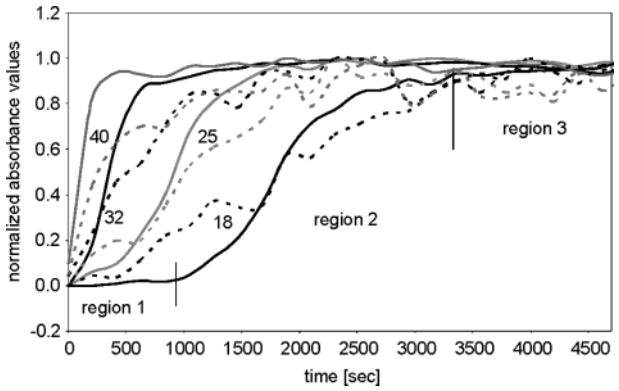

Figure 9. Profiles of the normalized integrated absorbance of the bands of s-PS corresponding to the crystalline s-PS (thin line) and of toluene (dotted line) as a function of solvent exposure time. The measurements were acquired with 210 s intervals. The numbers next to the lines show the corresponding FPA detector pixel number.

solvent present in the polymer, in that there is a minimum concentration of solvent required to initiate the crystallization process, and that the availability of solvent molecules has an influence on the crystallization kinetics. At 20 °C and 99.9% relative toluene vapor pressure, the near edge region crystallizes within 4 min. Therefore, rearrangements of macromolecular chains in the plasticized domains of s-PS cannot be supposed to be the rate limiting factor. Also, the transformation process from the amorphous glassy to amorphous plasticized form (plasticization) which is a prerequisite for crystallization occurs easily within this time range so that only the solvent diffusivity from the polymer surface to the solvent front within the polymer remains as a possible limiting and rate-determining factor. Solvent diffusivity may again be influenced by two parameters: the mobility of solvent molecules in the changed morphology of the crystalline polymer and the limited solvent flux on the polymer surface. In Figure 9 the integrated absorbance bands for δ-crystallinity and for toluene have been normalized and plotted for four horizontal pixel positions. Although the solvent data are noisy, it can be recognized in these averaged data that the slope of the dotted solvent curve is always shallower than the solid curve of the crystallinity band. This supports the hypothesis that solvent diffusivity is a key parameter and that a certain level of solvent must be present to initiate the crystallization process. Experiments to determine the amount of required solvent are continuing.

Conclusions

The application of FT-IR imaging to s-PS samples under controlled environments proved to be successful for studying solvent diffusion and induced crystallization. By restricting solvent diffusion to the direction perpendicular of the probing infrared beam, it was possible to follow the dynamic processes. Acquisition of FT-IR images in fixed time intervals, selective band integration, and subsequent plotting of integral absorbance values for each pixel of the FPA detector visualize the movement of solvent into the polymer and the extent of induced crystallinity. With the capabilities of transmission FT-IR imaging, spatially resolved spectral information for example from the polymer/solvent interface or areas in the bulk region could be obtained within a dynamic process time scale, highlighting the advantages of FT-IR imaging vs conventional single point and mapping experiments. Data from FT-IR images indicated Fickian diffusion behavior for toluene and provided diffusion coefficients at 20 and 35 °C.

Simultaneous and spatially resolved observations of the extent of s-PS crystallization at different distances from the polymer/solvent interface revealed details of the dependence of the crystallization on the solvent amount present. It was concluded that the amount of the solvent supplied at the polymer/solvent interface and diffusion of the solvent through the semicrystalline polymer are the rate determining factors in the crystallization process.

This study was focused on the assessment of solvent induced crystallization of polymers in a novel way utilizing the power of FT-IR imaging to study dynamic processes. We hope that this work will facilitate the use of spectroscopic imaging technology for polymer processing by revealing the underlying principles of polymer/solvent interactions.

Acknowledgment. The authors thank Dr. Helen Jervis (Surface Measurement Systems Ltd.) for help and advice, the Austrian Science Funds (FWF) for granting an Erwin Schrödinger visiting fellowship to Dr. Andreas Gupper (project: J2287-B10), and EPSRC (GR/S57600/01) for financial support.

References and Notes

(1) Lewis, E. N.; Treado, P. J.; Reeder, R. C.; Story, G. M.; Dowrey, A. E.; Marcott, C.; Levin, I. W. *Anal. Chem.* **1995**, *67*, 3377−3381.
(2) Bhargava, R.; Wang, S.-Q.; Koenig, J. L. *Appl. Spectrosc.* **1998**, *52*, 323−328.
(3) Gupper, A.; Wilhelm, P.; Schmied, M.; Kazarian, S. G.; Chan, K. L. A.; Reussner, J. *Appl. Spectrosc.* **2002**, *56*, 1515−1523.
(4) Fleming, O. S.; Chan, K. L. A.; Kazarian, S. G. *Vib. Spectrosc.* **2004**, *35*, 3−7.
(5) Chan, K. L. A.; Kazarian, S. G. *Appl. Spectrosc.* **2003**, *57*, 381−389.
(6) Vittoria, V. In *Handbook of Thermoplastics*; Olabisi, O., Ed.; Marcel Dekker: New York, 1997; pp 81−106.
(7) Guerra, G.; Vitagliano, V. M.; DeRosa, C.; Petraccone, V.; Corradini, P. *Macromolecules* **1990**, *23*, 1539−1544.
(8) Kellar, E. J. C.; Galiotis, C.; Andrews, E. H. *Macromolecules* **1996**, *29*, 3515−3520.
(9) Reynolds, N. M.; Hsu, S. L. *Macromolecules* **1990**, *23*, 3463−3472.
(10) Moyses, S.; Spells, S. J. *Macromolecules* **1999**, *32*, 2684−2689.
(11) Matsuba, G.; Kaji, K.; Nishida, K.; Kanaya, T.; Imai, M. *Macromolecules* **1999**, *32*, 8932−8937.
(12) Tashiro, K.; Ueno, Y.; Yoshioka, A.; Kobayashi, M. *Macromolecules* **2001**, *34*, 310−315.
(13) Tashiro, K.; Yoshioka, A. *Macromolecules* **2002**, *35*, 410−414.
(14) Yoshioka, A.; Tashiro, K. *Macromolecules* **2003**, *36*, 3593−3600.
(15) Yoshioka, A.; Tashiro, K. *Macromolecules* **2004**, *37*, 467−472.
(16) Chan, K. L. A.; Kazarian, S. G. *Vib. Spectrosc.* **2004**, *35*, 45−49.
(17) Kazarian, S. G.; Chan, K. L. A. *Macromolecules* **2004**, *37*, 579−584.
(18) Koenig, J. *Adv. Mater.* **2002**, *14*, 457−460.
(19) Ribar, T.; Bhargava, R.; Koenig, J. L. *Macromolecules* **2000**, *33*, 8842−8849.
(20) Miller-Chou, B. A.; Koenig, J. L. *Macromolecules* **2002**, *35*, 440−444.
(21) Snively, C. M.; Koenig, J. L. *J. Polym. Sci., Part B: Polym. Phys.* **1999**, *37*, 2261−2268.
(22) McDonald, P. J.; Godward, J.; Sackin, R.; Sear, R. P. *Macromolecules* **2001**, *34*, 1048−1057.

MA049313V